

# Temperature dependence of the static quark diffusion coefficient

Debasish Banerjee\*

*Saha Institute of Nuclear Physics, HBNI, Kolkata 700064, India and  
Homi Bhabha National Institute, Training School Complex, Anushaktinagar, Mumbai 400094, India*

Saumen Datta†

*Tata Institute of Fundamental Research, Homi Bhabha Road, Mumbai 400005, India*

Rajiv V. Gavai‡

*Indian Institute of Science Education and Research, Bhauri, Bhopal 462066, India*

Pushan Majumdar§

*Indian Association for the Cultivation of Science,  
Raja S. C. Mullick Road, Kolkata 700032, India*

The energy loss pattern of a low momentum heavy quark in a deconfined quark-gluon plasma can be understood in terms of a Langevin description. In thermal equilibrium, the motion can then be parametrized in terms of a single heavy quark momentum diffusion coefficient  $\kappa$ , which needs to be determined nonperturbatively. In this work, we study the temperature dependence of  $\kappa$  for a static quark in a gluonic plasma, with a particular emphasis on the temperature range of interest for heavy ion collision experiments.

PACS numbers:

## I. INTRODUCTION

The charm and the bottom quarks provide very important probes of the medium created in the relativistic heavy ion collision experiments. Since the masses of both of these quarks are much larger than the temperatures attained in RHIC and in LHC, one expects these quarks to be produced largely in the early pre-equilibrated state of the collision. Heavy quark probes therefore provide a window to look into the early stages of the fireball.

In particular, the nature of the interaction of the heavy quarks with the thermalized medium is different from that of the light quarks. For energetic jets radiative energy loss via bremsstrahlung is expected to be the dominant energy loss mechanism. For heavy quarks the radiative energy loss is suppressed in a cone of angle  $\sim m_Q/E$  [1]. For heavy quarks of moderate energy,  $E \lesssim 2m_Q$ , collision with thermal quarks and gluons is expected to be the dominant mechanism of energy loss [2, 3].

Even if the kinetic energy of the heavy quark is  $\mathcal{O}(T)$ , where  $T$  is the temperature of the fireball, its momentum will be much larger than the temperature. Its momentum is, therefore, changed very little in a single collision, and successive collisions can be treated as uncorrelated. Based on this picture, a Langevin description of the motion of the heavy quark in the medium has been proposed [4], [2, 3].  $v_2$ , the elliptic flow parameter, can then be calculated in terms of the diffusion coefficient of the heavy quark in the medium. The diffusion coefficient has been calculated in perturbation theory [2, 4]. While this formalism works quite well in explaining the experimental data for  $R_{AA}$  and  $v_2$  of the  $D$  mesons (see [5] for a review), the diffusion coefficient required to explain the data is found to be at least an order of magnitude lower than the leading order (LO) perturbation theory (PT) result.

This is not a surprise *per se*, as the quark-gluon plasma is known to be very nonperturbative at not-too-high temperatures and various transport coefficients have been estimated to have values very different from LOPT. However, this makes it important to have a nonperturbative estimate of the heavy quark diffusion coefficient. A field theoretic definition of the heavy quark diffusion coefficient to leading order of an  $1/M$  expansion was given in [6, 7]. Once again, the leading order perturbation theory results are very different from what is expected. The next-to-leading order (NLO) calculation [8] was found to change the LO result by nearly an order of magnitude at temperatures

---

\*Electronic address: debasish.banerjee@saha.ac.in

†Electronic address: saumen@theory.tifr.res.in

‡Electronic address: gavai@tifr.res.in

§Deceased.

$\lesssim 2T_c$ . While the NLO results are in the direction suitable for explaining the experimental data, the large change from LO to NLO indicates an inadequacy of perturbation theory in obtaining a reliable estimate for the diffusion coefficient in the temperature range of interest, and makes a nonperturbative estimate essential.

The first nonperturbative results for  $\kappa$ , using the formalism of [7] and numerical lattice QCD in the quenched approximation (i.e., gluonic plasma), supported a value of  $\kappa$  substantially different from LOPT and in the correct ballpark for HIC phenomenology [9]. Of course, the plasma created in experiments is not a gluonic plasma, and one needs a full QCD calculation for phenomenology; but the fact that the quenched QCD result is of right order of magnitude gives strong support for the Langevin description of the heavy quark energy loss. Later works [10–12] improved on the calculations of [9]. In particular, [10, 12] conducted a study at  $1.5 T_c$ , and explored various systematics like discretization effects and the extraction of  $\kappa$ . The focus of Ref. [11] was in comparison with perturbation theory, and asymptotically high temperatures were explored. Meanwhile, a nonperturbative definition of the first correction to the static limit was discussed in [13]. Nonperturbative estimates of this correction have recently been carried out [14, 15].

In this work we have carried out a study of the static quark momentum diffusion coefficient  $\kappa$  in the temperature range  $\lesssim 3.5T_c$ , following the formalism of [7]. The focus here is on studying the change of  $\kappa$  with temperature. We extend the temperature range studied in [9] to cover the entire temperature range of interest to the heavy ion community, but also improve the analysis technique, following [14] (which incorporates the analysis of [10]). After explaining the formalism in Section II, in Section IV we present the results of our study. Combined with the  $1/M$  correction terms calculated in [9], this gives the results for momentum diffusion coefficients for the charm and the bottom.

## II. LANGEVIN FORMALISM AND NONPERTURBATIVE DEFINITION OF THE MOMENTUM DIFFUSION COEFFICIENT $\kappa$

In this section, we outline the formalism underlying our study. We first define the Langevin formalism for the heavy quark energy loss, as described in [4], [2, 3], and then outline the nonperturbative definition of the diffusion coefficient, following [6, 7].

The heavy quark momentum is much larger than the system temperature: even for a near-thermalized heavy quark with kinetic energy  $\sim T$ ,  $p_Q \sim \sqrt{MT}$ . Individual collisions with the medium constituents with energy  $\sim T$  do not change the momentum of the heavy quark substantially. Therefore, the motion of the heavy quark is similar to a Brownian motion, and the force on it can be written as the sum of a drag term and a “white noise”, corresponding to uncorrelated random collisions:

$$\frac{dp_i}{dt} = -\eta_D p_i + \xi_i(t), \quad \langle \xi_i(t) \xi_j(t') \rangle = \kappa \delta_{ij} \delta(t - t'). \quad (1)$$

The momentum diffusion coefficient,  $\kappa$ , can be obtained from the correlation of the force term:

$$\kappa = \frac{1}{3} \int_{-\infty}^{\infty} dt \sum_i \langle \xi_i(t) \xi_i(0) \rangle. \quad (2)$$

The drag coefficient,  $\eta_D$ , can be connected to the diffusion coefficient using standard fluctuation-dissipation relations [16]:

$$\eta_D = \frac{\kappa}{2MT}. \quad (3)$$

Here  $M$  is the heavy quark mass.

In the leading order in an expansion in  $\frac{1}{m_Q}$  the heavy quark interacts only with the color electric field of the plasma. Therefore the momentum diffusion coefficient  $\kappa$  can be obtained from the electric field correlation function [6, 7]

$$G_{EE}(\tau) = -\frac{1}{3} \sum_{i=1}^3 \frac{\langle \Re \text{Tr} (U(\beta, \tau) gE_i(\tau, \vec{x}) U(\tau, 0) gE_j(0, \vec{x})) \rangle}{\langle \Re \text{Tr} U(\beta, 0) \rangle}. \quad (4)$$

where  $U(\tau_1, \tau_2)$  is the gauge link in Euclidean time from  $\tau_1$  to  $\tau_2$  and  $E(\tau)$  is the color electric field insertion at Euclidean time  $\tau$  (see [7] for a formal derivation).

The spectral function,  $\rho_T(\omega)$ , for the force term is connected to  $G_{EE}$  by the integral equation [16]

$$G_{EE} = \int_0^\infty \frac{d\omega}{\pi} \rho_T(\omega) \frac{\cosh \omega(\tau - \frac{1}{2T})}{\sinh \frac{\omega}{2T}}. \quad (5)$$

The momentum diffusion coefficient,  $\kappa_E$  is then given by

$$\kappa_E = \lim_{\omega \rightarrow 0} \frac{2T}{\omega} \rho_T(\omega). \quad (6)$$

In this work we will use eq. (5), eq. (6) to calculate the momentum diffusion coefficient  $\kappa_E$  for moderately high temperatures  $T \lesssim 3.5T_c$ . In particular, we will be exploring the temperature dependence of  $\kappa_E/T^3$ .

Note that  $\kappa_E$  is the leading order estimate of  $\kappa$  in an  $1/m_Q$  expansion. The  $\mathcal{O}(m_Q^{-1})$  correction has been explored [13]: modulo some approximations, one can write

$$\kappa \approx \kappa_E + \frac{2T}{M_{\text{kin}}} \kappa_B \quad (7)$$

where  $\kappa_B$  is the estimate of the diffusion coefficient one gets by replacing the electric fields with magnetic fields in eq. (5) and eq. (6), and has been calculated in Ref. [14] for the gluonic plasma.

### III. OUTLINE OF THE CALCULATION

We calculated the electric field correlator  $G_{EE}$ , eq. (4), for gluonic plasma using lattice discretization and numerical Monte Carlo techniques. On the lattice, the electric field was discretized, following [7], as

$$E_i(\vec{x}, \tau) = U_i(\vec{x}, \tau) U_4(\vec{x} + \hat{i}, \tau) - U_4(\vec{x}, \tau) U_i(\vec{x} + \hat{4}).$$

Then the lattice discretized  $EE$  correlator takes the form

$$G_{EE}^{\text{bare}}(\tau) = \frac{C^i(\tau+1) + C^i(\tau-1) - 2C^i(\tau)}{\prod_{x_4=0}^{\beta} U_4(x_4)}$$

$$C^i(\tau) = \prod_{x_4=0}^{t-1} U_4(x_4) \cdot E_i(t) \cdot \prod_{x_4=t}^{t+\tau-1} U_4(x_4) \cdot E_i(t+\tau) \cdot \prod_{x_4=t+\tau}^{\beta-1} U_4(x_4). \quad (8)$$

The bare correlator  $G_{EE}^{\text{bare}}(\tau)$  is ultraviolet finite: on the lattice, it only has a finite  $a$  renormalization constant  $Z_E(g^2(a), a) \rightarrow 1$  as  $a \rightarrow 0$ .

We have calculated the correlators  $G_{EE}^{\text{bare}}$  on the lattice at various temperatures  $\lesssim 3.5T_c$ . Equilibrium configurations for a gluonic plasma were generated at various temperatures by using lattices with temporal extent  $N_\tau(\beta) = \frac{1}{T a(\beta)}$ ,

where  $\beta = \frac{6}{g^2}$  is the coefficient of the plaquette term in the Wilson gauge action. The details of the lattices generated and the number of configurations at each parameter set is given in Table I.

The spatial extent of the lattices are chosen such that  $LT > 3$  and also the lattice is confined in the spatial direction. At various temperatures we have more than one lattice spacings; this allows us to estimate the discretization error, and to get the continuum result. Also for various values of the coupling, we have changed  $N_\tau$  to change the temperature, keeping all the other parameters of the lattice unchanged. A comparison of the results from such lattices give us a direct handle on the temperature modification of  $\kappa_E$ .

Since we require very accurate correlation functions on lattices with large temporal extents, we have used the multilevel algorithm [17] in calculating eq. (8). The implementation of the algorithm is outlined in [9], which we follow. The number of sublattices for the multilevel update, and the number of sublattice updates, are shown in Table I, where each update consisted of (1 heatbath+3 overrelaxation) steps. Typically, a number of parallel runs with independent random number seeds were used at each parameter sets. After a thermalization run which is many times the autocorrelation length,  $\mathcal{O}(100)$  configurations were generated from each stream. The total number of configurations generated is shown in Table I.

TABLE I: Summary of runs and statistics.

$\beta$	$N_\tau$	$N_\sigma$	$T/T_c$	# sublattice	# update	# conf
7.05	20	64	1.50	5	500	1270
7.192	24	72	1.48	4	2000	2032
7.30	20	64	2.03	5	500	1200
7.457	24	80	2.04	4	500	1000
	20	80	2.45	6	500	730
7.634	30	96	2.01	5	2000	640
	24	96	2.51	4	2000	657
	20	96	3.01	5	2000	500
7.78	28	96	2.55	7	2000	678
	24	96	2.98	4	2000	536
	20	96	3.55	5	2000	522
7.909	28	96	2.96	7	2000	1100
	24	96	3.46	6	2000	967

The temperature scale shown in Table I is obtained from the interpolation formula [18]

$$\log \frac{r_0}{a} = \left[ \frac{\beta}{12b_0} + \frac{b_1}{2b_0^2} \log \frac{6b_0}{\beta} \right] \frac{1 + c_1/\beta + c_2/\beta^2}{1 + c_3/\beta + c_4/\beta^2} \quad (9)$$

where  $b_0 = 11/(4\pi)^2$  and  $b_1 = 102/(4\pi)^4$ . The fit parameters  $c_i$  are

$$c_{\{1,2,3,4\}} = \{-8.9664, 19.21, -5.25217, 0.606828\} \quad (10)$$

and  $r_0 T_c = 0.7457$  [18]. Other ways of determining the temperature gives slightly different values: e.g., using [19] leads to a temperature which differs by  $\sim 1$ -1.5% at the higher  $\beta$  values of Table I. So we will effectively round off the temperature and, e.g., treat 3.46  $T_c$  and 3.55  $T_c$  in Table I as  $\sim 3.5 T_c$ .

#### IV. ANALYSIS OF THE CORRELATORS AND EXTRACTION OF $\kappa/T^3$

##### A. Discretization effect in $G_{EE}^{\text{bare}}$

The  $EE$  correlation functions  $G_{EE}$  are ultraviolet finite. The bare correlators  $G_{EE}^{\text{bare}}$  have only finite renormalization:

$$G_{EE}^{\text{renorm}} = Z_{EE}(a) G_{EE}^{\text{bare}}. \quad (11)$$

The renormalization coefficient  $Z(a)$  has been determined at one loop level in [20]:

$$Z_{EE} = 1 + \frac{2g_B^2 C_f}{3} P_1 \approx 1 + 0.1377 g_B^2 \quad (12)$$

where the lattice bare coupling  $g_B^2 = 6/\beta$ ,  $C_f = \frac{4}{3}$ , and  $P_1 = \int_{-\pi}^{\pi} \frac{d^4 k}{(2\pi)^4} \frac{1}{K^2} \approx 0.15493$ .

After the renormalization, the correlator still shows cutoff effect, especially at short distances. A major part of this cutoff effect at short distances can be taken into account by a consideration of the discretization effect in the leading order. In leading order, the  $EE$  correlator takes the form [21]

$$G_{EE}(\tau, LO) = g^2 C_f G_{\text{norm}}(\tau), \quad (13)$$

$$G_{\text{norm}}^{\text{Cont}}(\tau) = \pi^2 T^4 \text{cosec}^2(\pi\tau T) \left( \cot^2(\pi\tau T) + \frac{1}{3} \right) \quad (14)$$

$$G_{\text{norm}}^{\text{Lat}}(\tau) = \frac{1}{3a^4} \int \frac{d^3 k}{8\pi^3} \frac{e^{\bar{k}(N_\tau - t)} + e^{\bar{k}t}}{e^{\bar{k}N_\tau} - 1} \frac{\tilde{k}^2}{\sinh \bar{k}} \quad (15)$$

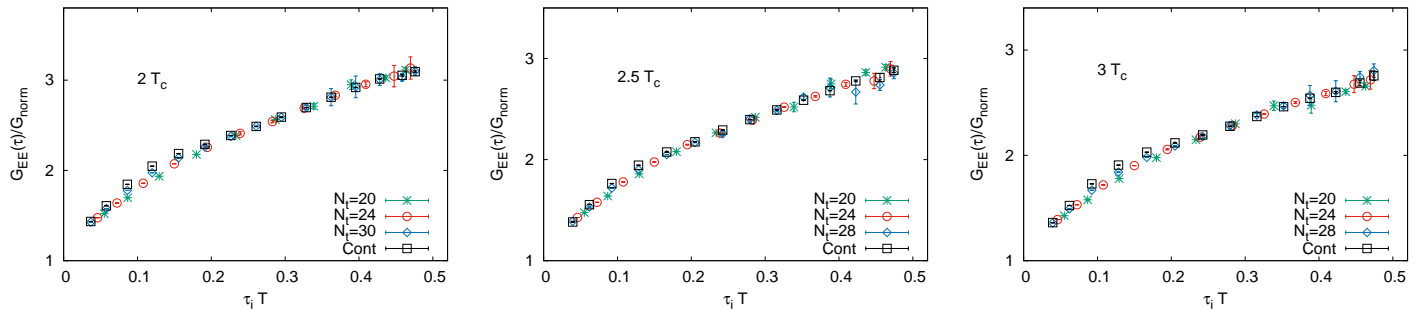


FIG. 1: Continuum extrapolation of the correlator ratio  $\frac{G_{EE}(\tau)}{G_{norm}}(\tau)$ , at (left)  $2 T_c$ . (middle)  $2.5 T_c$  and (right)  $3 T_c$ .

where the integration is over the Brillouin zone  $(-\pi, \pi)$  and

$$\frac{\bar{q}}{2} = \operatorname{arcsinh} \frac{\tilde{q}}{2}, \quad \tilde{q}^2 = \sum_{i=1}^3 4 \sin^2 \frac{q_i}{2}. \quad (16)$$

A major part of the discretization effect can be accounted for by a comparison of eq. (14) with eq. (15): in particular, by defining an *improved distance*  $t_{\text{imp}}$  through [21, 22]

$$G_{\text{norm}}^{\text{Lat}}(t_{\text{imp}}) = G_{\text{norm}}^{\text{Cont}}(\tau). \quad (17)$$

We have  $G_{EE}^{\text{bare}}$  at multiple lattice spacings at each temperature. As noted in [10, 11] before, we found that the use of  $t_{\text{imp}}$ , eq. (17), reduces considerably the short distance discretization effect in  $G_{EE}^{\text{bare}}$ . In what follows, we have used  $t_{\text{imp}}$  to denote the distance scale for  $G_{EE}^{\text{renorm}}$ .

At  $T/T_c = 2, 2.5$  and  $3$  we have three lattice spacings each. Using these correlators, we find the continuum extrapolated correlators at distances corresponding to  $t_{\text{imp}}$  for the finest lattice. We extrapolate  $\frac{G_{EE}}{G_{norm}}(\tau)$  to  $a \rightarrow 0$ , where  $G_{norm} = G_{norm}^{\text{Lat}}$ , and  $\tau$  takes the values  $t_{\text{imp}}$  of the finest lattice at each temperature. The method is explained in Appendix A. The results of the extrapolation for  $\frac{G_{EE}}{G_{norm}}(\tau)$  is shown in Figure 1. The extrapolated ratio is now multiplied by  $G_{norm}(\tau)$  to get the continuum extrapolated correlator. We perform a bootstrap analysis, by first blocking the data in blocks of size at least 2-3 times the autocorrelation time.

It is interesting to compare the continuum extrapolated correlator with perturbation theory.  $G_{EE}$  has been calculated in perturbation theory to NLO in Ref. [23]. In Figure 2 we compare the perturbative results of Ref. [23] with our nonperturbatively determined correlator. In Ref. [23] the scale for the running coupling has been set at

$$\mu_{\text{opt}} \approx \max[7.57\omega, 6.74T]. \quad (18)$$

following the *principle of minimal sensitivity*. The LO and NLO bands in Figure 2 are obtained by varying  $\mu \in [0.5, 2]\mu_{\text{opt}}$ . This way of scale setting leads to a good agreement between the LO and the NLO calculation; but as Figure 2 shows, the perturbative estimates are very different from the nonperturbative results. We also show the LO results obtained by setting the scale in an intuitive way [10]:

$$\mu_{\text{fit}} = \max[\omega, \pi T]. \quad (19)$$

The band is obtained by varying this scale by a factor  $[0.5 - 2.0]$  as before. As Figure 2 shows, the LO curve captures the main features of the nonperturbative result. However, the good agreement of perturbation theory with the lattice result in this case is misleading, as the NLO result changes strongly from the LO result and the lattice result. Heartened by Figure 2, We will still use this scale for modelling the ultraviolet part of the spectral function.

## B. Extraction of $\kappa$ from the correlators

A direct inversion of eq. (5) to get  $\rho_T(\omega)$  is very difficult. Instead, to get an estimate of what kind of  $\kappa_E$  is consistent with the  $G_{EE}$  obtained, we have used some simple models for  $\rho_T(\omega)$ . Our models, and the analysis strategy, are similar

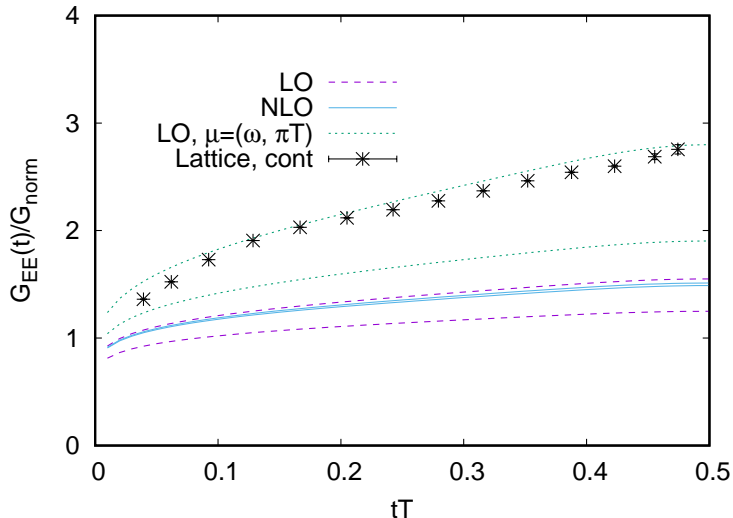


FIG. 2: A comparison of the nonperturbatively obtained correlator  $\frac{G_{EE}}{G_{norm}}(\tau)$  with the results of perturbation theory [23]. The LO and NLO results use an optimized scale (eq. (18)). Also shown is the LO result with the scale  $\mu = \max[\omega, \pi T]$  (eq. (19)). In each case, the bands for the perturbation theory are obtained by varying the scale by a factor of two in each direction from the scale mentioned above.

to what was followed in [14] for  $G_{BB}(\tau)$ , which, in turn, was influenced by earlier works [9, 10] on  $G_{EE}$ . The ultraviolet and the infrared parts of  $\rho_T(\omega)$  are modelled with the simple forms

$$\rho_{UV}(\omega) = \frac{g^2(\mu_{\text{fit}}) C_f \omega^3}{6\pi}, \quad \rho_{IR}(\omega) = \kappa_E \omega, \quad (20)$$

where  $\mu_{\text{fit}}$  is defined in eq. (19).  $\rho_{IR}(\omega)$  is the simplest form capturing the dissipative behavior of  $\kappa_E$ . The correlator eq. (4) does not have a transport peak, and is expected to have a smooth linear behavior in the infrared [7, 23], motivating  $\rho_{IR}(\omega)$ .  $\rho_{UV}(\omega)$  is the known leading order form of the spectral function and the scale choice is motivated by Figure 2. The NLO spectral function is known [23] but, as Figure 2 shows, it is not clear that it will capture the ultraviolet behavior better except at very high  $\omega$ .

While both  $\rho_{UV}(\omega)$  and  $\rho_{IR}(\omega)$  are well-motivated, not much is known *a-priori* about the form of the spectral function in the intermediate  $\omega$  regime. An ansatz, that allows  $\rho_T(\omega)$  to continuously change from  $\rho_{UV}(\omega)$  to  $\rho_{IR}(\omega)$ , is

$$\rho_T(\omega) = \max[c\rho_{UV}(\omega), \rho_{IR}(\omega)] \quad (21)$$

where we have introduced a parameter  $c$  to take into account uncertainty due to scale choice and the use of the leading order form for  $\rho_{UV}(\omega)$ .  $c$  is treated as a fit parameter. The best fit values we obtained for  $c$  are close to 1, in the range 1-1.2.

A more smooth form of connecting  $\rho_{UV}(\omega)$  with  $\rho_{IR}(\omega)$  is

$$\rho_T(\omega) = \left[ \sqrt{(c\rho_{UV}(\omega))^2 + \rho_{IR}(\omega)^2} \right]. \quad (22)$$

The form of eq. (22) has been considered theoretically better justified in [10], [12]. Here again, the fit parameter  $c \sim 1$  is introduced to account for uncertainty in  $\rho_{UV}(\omega)$ . In our analysis we have treated eq. (21) and eq. (22) at par.

Instead of introducing a fit parameter  $c$  as above, ref. [10] has suggested parametrizing the difference between the above form (with  $c=1$ ) and  $\rho_T(\omega)$  in a sine expansion:

$$\left( 1 + \sum_n c_n \sin(\pi n y) \right), \quad y = \frac{x}{1+x}, \quad x = \log\left(1 + \frac{\omega}{\pi T}\right).$$

For the fit range we used, we found that one term in the expansion sufficed to fit our correlator. Therefore we have also tried the fit forms

$$\rho_T(\omega) = (1 + c_1 \sin \pi y) \left[ \sqrt{\rho_{UV}(\omega)^2 + \rho_{IR}(\omega)^2} \right]; \quad (23)$$

$$= (1 + c_1 \sin \pi y) \max[\rho_{UV}(\omega), \rho_{IR}(\omega)]. \quad (24)$$

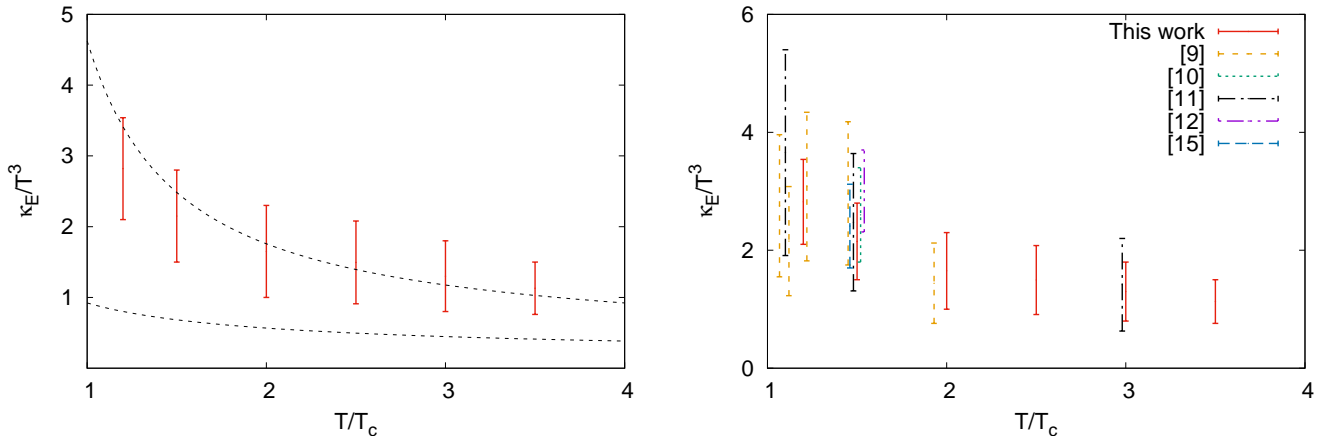


FIG. 3: (Left) Our estimates for the range of  $\kappa_E/T^3$  in the temperature range  $\lesssim 3.5T_c$ . Also shown is the NLO perturbation theory estimate eq. (25) [8]; the band corresponds to varying the scale of the coupling  $g^2(\mu)$  in the range  $\mu \in [\pi T, 4\pi T]$ . (Right) A survey of other existing lattice results for  $\kappa_E$  in gluonic plasma in the 1-4  $T_c$  temperature range. For visual clarity, points at  $1.5 T_c$  and  $3 T_c$  have been slightly shifted horizontally.

TABLE II: Temperature dependence of  $\kappa_E/T^3$

$T/T_c$	1.2	1.5	2.0	2.5	3.0	3.5
$\kappa_E/T^3$	2.1 - 3.5	1.5 - 2.8	1.0 - 2.3	0.9 - 2.1	0.8 - 1.8	0.75 - 1.5

In all our fits we have found  $c_1$  to be small,  $\in [0.02, 0.12]$ .

We perform the whole analysis for each of the forms of the model above in a bootstrap framework. Our final estimates of  $\kappa_E$  are shown in Table II and in Figure 3. The details of the analysis can be found in Appendix A, where the estimates for each model are given in Table III and Figure 6. Our estimates in Table II and Figure 3 include the entire bands for eq. (22), eq. (21) and the central values for eq. (23), eq. (24).

There are other estimates of  $\kappa_E/T^3$  for gluonic plasma from the lattice. While our paper [9] studied the temperature range close to  $T_c$ , a detailed study at  $1.5 T_c$  was performed in [10]. A broad temperature range was studied in [11], but with the main focus being very high temperatures. While the analysis techniques, in particular the spectral function models, vary, all these references used multilevel algorithm and perturbative renormalization constants. Recently, [12] and [15] have used gradient flow [24] to get renormalized  $EE$  correlators at  $1.5 T_c$ . We compare these studies with ours in the right panel of Figure 3. Within the large uncertainties of our and other studies, our results agree very well with the other studies.

## V. SUMMARY AND DISCUSSION

In this paper we have studied the electric field correlator, eq. (4), in a thermally equilibrated gluonic plasma at moderately high temperatures  $T \lesssim 3.5T_c$ . We investigated in detail the cutoff dependence of the correlators, and took the continuum limit (Figure 1). With a simple set of models for the  $EE$  spectral function  $\rho_T(\omega)$ , we then estimated the static quark momentum diffusion coefficient  $\kappa_E$ . The results are shown in Figure 3 and in Table II.

$\kappa_E/T^3$  has been calculated to NLO in perturbation theory in [8]. For SU(3) gluonic plasma, the NLO result is

$$\kappa_E/T^3 = \frac{g^4 C_F}{6\pi} T^3 \left[ \log \frac{2T}{m_D} + \xi + C g \right] \quad (25)$$

where  $C_F = 4/3$ ,  $\xi \approx -0.64718$ ,  $C \approx 2.3302$  and  $m_D = gT$  in LO perturbation theory. This NLO result is shown in Figure 3, where the band corresponds to evaluating  $g^2$  at the scales  $\mu \in [\pi T, 4\pi T]$ . The NLO results explain the data quite well. Note, however, that perturbation theory is inherently unstable here: the LO result is an order-of-magnitude smaller than NLO. In fact, if we omit the  $\mathcal{O}(g)$  term in eq. (25), we will get a negative value for  $\kappa_E/T^3$

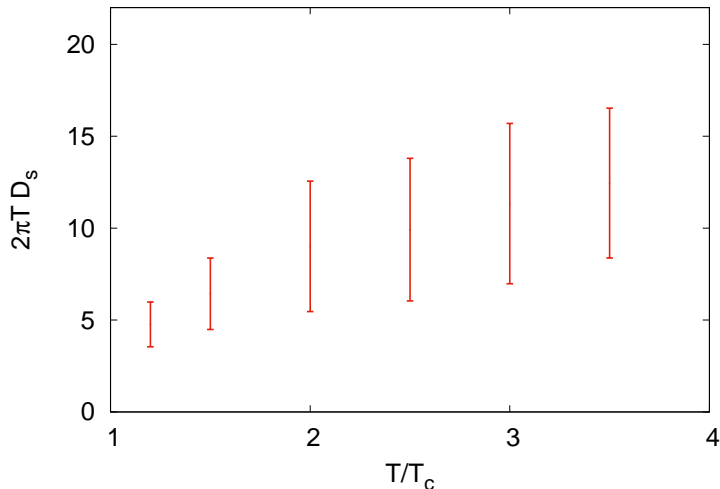


FIG. 4: An estimation of the static quark diffusion coefficient, using eq. (26) and Table II.

in our temperature range [23]. The agreement of the NLO result with the nonperturbative results may indicate that the corrections beyond NLO are small.

While it is the momentum diffusion coefficient that enters the equations of Langevin dynamics and is of interest for the phenomenology of heavy quark thermalization, it has been the convention to quote the transport coefficient as the position space diffusion coefficient  $D_s$ . In particular, the combination

$$2\pi T D_s = \frac{4\pi}{\kappa/T^3} \quad (26)$$

is usually quoted. In the left panel of Figure 4 we plot  $2\pi T D_s$  as obtained from our results of  $\kappa_E$  using eq. (26).

$2\pi T D_s$  shows a rising trend with temperature. The temperature dependence of  $2\pi T D_s$  is of great interest to phenomenological studies [25–27]. In such studies, a parametric temperature dependence of

$$2\pi T D_s \sim \alpha + \beta \left( \frac{T}{T_c} - 1 \right) \quad (27)$$

is sometimes used [26]. Our data is consistent with such a dependence (admittedly, aided by the large uncertainties in our measurements), with  $\alpha = 4.27(29)$  and  $\beta = 3.60(33)$  [28]. We also tried doing this linear fit for  $2\pi T D_s$  from each of the models of Section IV B. The results can be seen in Figure 7 and Table IV in Appendix A. All of the model spectral functions indicate a positive slope of  $2\pi T D_s$  with temperature. We emphasize that eq. (27) is a purely phenomenological fit: the temperature dependence of  $D_s$  is of course more complicated, e.g., eq. (25).

## VI. ACKNOWLEDGEMENTS

We thank Mikko Laine for providing the perturbative curves in Figure 2, and for discussions. The computations presented in this paper were performed on the clusters of the Department of Theoretical Physics, TIFR, and on the ILGTI computing facilities of IACS and TIFR. We would like to thank Ajay Salve and Kapil Ghadiali for technical assistance. S.D. acknowledges support of the Department of Atomic Energy, Government of India, under Project Identification No. RTI 4002.

### Appendix A: Some details of the numerical analysis

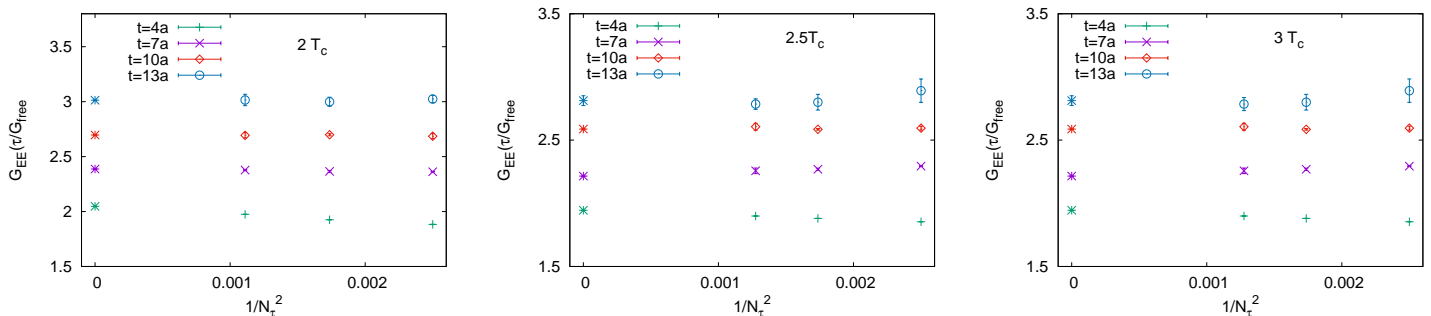
Here we provide additional details of our numerical analysis in Section IV.

Our whole analysis is done in a bootstrap formalism. To get the continuum correlator, the average correlator for each bootstrap sample is B-spline interpolated, and the value of the correlation function at distances corresponding



TABLE III: Results for  $\kappa_E/T^3$  from the different fit forms of Section IV B.

$T/T_c$	eq. (21)	eq. (22)	eq. (24)	eq. (23)
1.2	2.16-2.80	2.44-3.54	1.80-2.50	2.34-3.14
1.5	1.74-2.16	1.62-2.80	1.25-1.73	1.55-2.27
2	1.05-1.60	1.48-2.30	0.77-1.42	1.04-1.82
2.5	0.91-1.77	1.17-2.08	0.70-1.59	0.97-1.86
3	0.87-1.48	1.04-1.80	0.60-1.30	0.83-1.56
3.5	0.76-1.14	1.01-1.50	0.62-1.02	0.96-1.33

FIG. 5: Illustration of the continuum extrapolation of the correlator normalized by  $G_{norm}$ . (Left)  $2 T_c$ , (middle)  $2.5 T_c$  and (right)  $3 T_c$ .

to the  $t_{imp}$  values of the finest lattice are obtained. Note that this typically involves an *extrapolation* at the smallest distance, but this is not a concern as this distance is not used in the fits. A very slight extrapolation is also required at the largest ( $t \sim 1/2T$ ) distance point, but it is a very small extrapolation and we do not expect this to be a problem.

At short distances  $t_i T \lesssim 0.15$  we see a clear discretization effect, which is approximately linear in  $a^2$ ; we fit to a linear form to get the continuum correlator. For larger distances  $t_i T > 0.25$  the correlators do not show a clear discretization effect. In particular, for correlators at large distances  $t_i T \gtrsim 0.3$  we found a constant fit to be more reasonable. We show examples of our continuum extrapolation at some representative distances in Figure 5. Note that we have also carried out the analysis with linear extrapolation at all distances; the  $\kappa$  values obtained agree within errorbar.

To extract  $\kappa_E$  from the continuum correlators using eq. (5), we have used the fit forms discussed in Section IV B, and done a standard  $\chi^2$  fit. The [16,84] percentile band of the bootstrap estimators of  $\kappa_E$  is treated as the  $1\text{-}\sigma$  errorband. The results for the various fit forms are shown in Figure 6. Typically we get a good  $\chi^2$  by taking the whole range except the two shortest distance points. We have, however, also varied  $t_{imp}^{\min}$ . The results shown in Figure 6 include the variation with fit range, and any difference due to using linear vs constant extrapolation at large separations in Figure 5.

As mentioned in Section IV B, we have also fitted the correlators from the individual lattices to the forms of Section IV B. For this we have used  $t_{imp}^{\min} \sim 0.25/T$ , where the discretization effect on the correlators is small.  $t_{imp}^{\min}$  is further varied within a small range. The bands shown in Figure 6 include spread due to such a variation.

In Table III we show the final results for  $\kappa_E/T^3$  using the different fit forms. The error estimate is conservative, covering the  $1\sigma$  interval obtained from the continuum correlator and the correlators from lattices with  $N_t \geq 24$ .

Table III also includes two temperatures where we have only two lattice spacings each, and  $1.2 T_c$  where we have just  $N_t=24$ . In these cases we have only fitted the individual lattices. The rest of the discussion is the same as above. The final result in these cases is taken from the  $N_t=24$  lattices.

For the final result for  $\kappa_E$  shown in Figure 3, we have treated the fit forms eq. (21) and eq. (22) at par, and conservatively quoted an error band that includes the bands for eq. (21) and eq. (22) in Table III and the central values of the bands for eq. (21) and eq. (22). These results are also shown in Table II.

Using Table III and eq. (26) we can also make separate estimates for  $2\pi T D_s$  for each form of the model  $\rho_T(\omega)$  in Section IV B. This is shown in Figure 7. The linearly rising behavior of each of these forms can then be separately

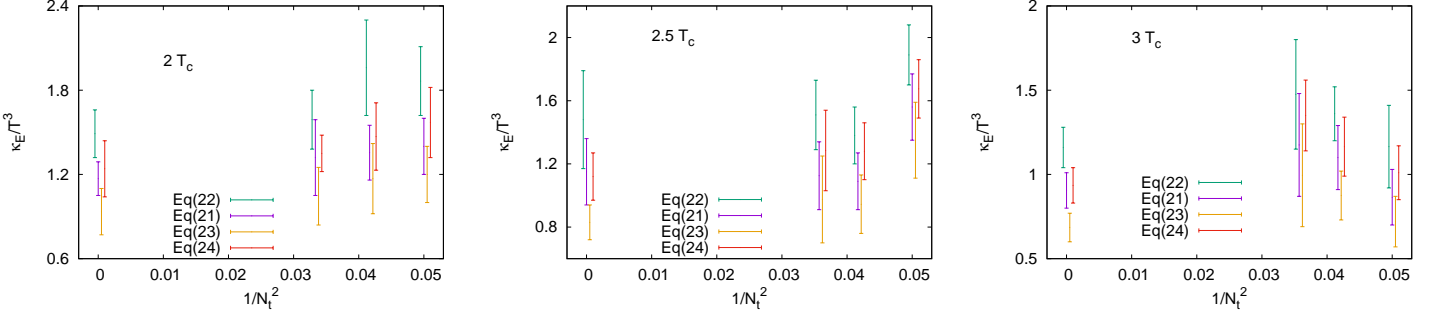


FIG. 6: Results for  $\kappa_E/T^3$  obtained at  $T/T_c = 2$  (left), 2.5 (middle) and 3 (right). Besides the continuum results, the results obtained from fitting individual lattices is also shown. See the text for details of the error band.

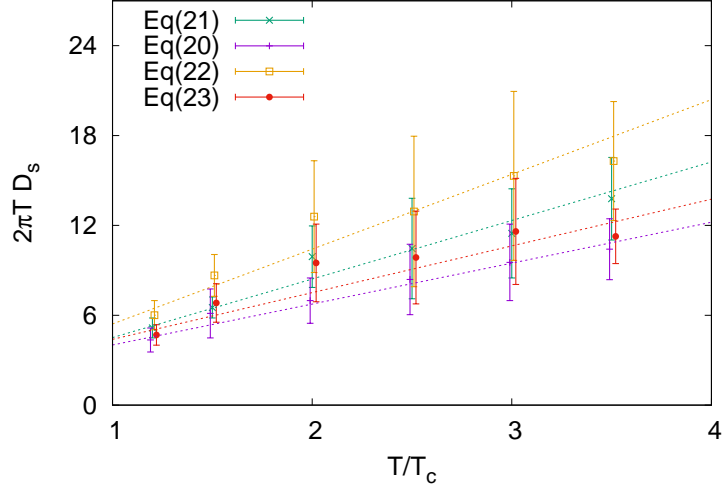


FIG. 7: An estimation of the static quark diffusion coefficient, using eq. (26) and Table II. Also shown are the best fits to a linear temperature dependence (eq. (27)).

fitted to the linear fit form eq. (27). The results of such a fit are shown in Table IV.

- 
- [1] Y. Dokshitzer & D. Kharzeev, *Phys. Lett. B* 519 (2001) 199.
  - [2] G. D. Moore and D. Teaney, *Phys. Rev. C* 71 (2005) 064904.
  - [3] M. G. Mustafa, *Phys. Rev. C* 72 (2005) 014905.
  - [4] B. Svetitsky, *Phys. Rev. D* 37 (1988) 2484.
  - [5] X. Dong, Y-J. Lee & R. Rapp, *Ann. Rev. Nucl. Part. Sci.* 69 (2019) 417.
  - [6] J. Casalderrey-Solana and D. Teaney, *Phys. Rev. D* 74 (2006) 085012.

TABLE IV: The fit parameters for eq. (27)

	eq. (22)	eq. (21)	eq. (23)	eq. (24)
$\alpha$	4.01(24)	4.51(27)	5.42(50)	4.39(45)
$\beta$	3.91(39)	2.73(24)	4.99(71)	3.12(50)

- [7] S. Caron-Huot, M. Laine & G. Moore, *J. H. E. P.* 04 (2009) 053 (0901.1195).
- [8] S. Caron-Huot & G. Moore, *J. H. E. P.* 0802 (2008) 081.
- [9] D. Banerjee, S. Datta, R. Gavai & P. Majumdar, *Phys. Rev. D* 85 (2012) 014510 (1109.5738).
- [10] A. Francis, O. Kaczmarek, M. Laine, T. Neuhaus & H. Ohno, *Phys. Rev. D* 92 (2015) 116003.
- [11] N. Brambilla, V. Leino, P. Petreczky & A. Vairo, *Phys. Rev. D* 102 (2020) 074503.
- [12] L. Altenkort, A. Eller, O. Kaczmarek, L. Mazur, G. Moore & H.-T. Shu, *Phys. Rev. D* 103 (2021) 014511.
- [13] A. Buttefeux and M. Laine, *J. H. E. P.* 12 (2020) 150.
- [14] D. Banerjee, S. Datta & M. Laine, arXiv:2204.14075.
- [15] N. Brambilla, V. Leino, J. Mayer-Steudte & P. Petreczky, arXiv:2206.02861.
- [16] J. Kapusta & C. Gale, *Finite Temperature Field Theory: Principles and Applications*, 2nd Edition. Cambridge University Press, 2006.
- [17] M. Lüscher and P. Weisz, *J. H. E. P.* 0109 (2001) 010, *J. H. E. P.* 0207 (2002) 049.
- [18] Y. Burnier, H-T. Ding, O. Kaczmarek, A-L. Kruse & M. Laine, *J. H. E. P.* 11 (2017) 206.
- [19] R.G. Edwards, U.M. Heller & T.R. Klassen, *Nucl. Phys. B* 517 (1998) 377
- [20] C. Christensen & M. Laine, *Phys. Lett. B* 755 (2016) 316 (1601.01573).
- [21] A. Francis, O. Kaczmarek, M. Laine & J. Langelage, PoS LATTICE2011 (arXiv:1109.3941).
- [22] R. Sommer, *Nucl. Phys. B* 411 (1994) 839.
- [23] Y. Burnier, M. Laine, J. Langelage, L. Mether, *J. H. E. P.* 08 (2010) 094
- [24] M. Lüscher, *J. H. E. P.* 08 (2010) 071.
- [25] S. Cao, *et al.*, *Phys. Rev. C* 99 (2019) 054907.
- [26] Y. Xu, J. Bernhard, S. Bass, M. Nahrgang & S. Cao, *Phys. Rev. C* 97 (2018) 014907.
- [27] S. K. Das, F. Scardina, S. Plumari & V. Greco, *Phys. Lett. B* 747 (2015) 260.
- [28] For this fit we have done a simple  $\chi^2$  analysis, treating the error band in Table II as a statistical  $1\sigma$  band. The error band in the table is actually dominated by systematic errors. So while the fit does indeed indicate that the data is inconsistent with a flat behavior with temperature, one should not attribute the standard  $1\sigma$  interpretation to the error bar quoted for the fit parameters.

